Spin waves in the two-dimensional honeycomb lattice XXZ-type van der Waals antiferromagnet $CoPS_3$

Chaebin Kim,[1,2,3] Jaehong Jeong,[2,3,*] Pyeongjae Park,[1,2,3] Takatsugu Masuda,[4] Shinichiro Asai,[4] Shinichi Itoh,[5] Heung-Sik Kim,[6] Andrew Wildes,[7] and Je-Geun Park[1,2,3,†]

[1]*Center for Quantum Materials, Seoul National University, Seoul 08826, Korea*
[2]*Center for Correlated Electron Systems, Institute for Basic Science, Seoul 08826, Korea*
[3]*Department of Physics and Astronomy, Seoul National University, Seoul 08826, Korea*
[4]*Institute for Solid State Physics, The University of Tokyo, Chiba 277-8581, Japan*
[5]*Institute of Materials Structure Science, High Energy Accelerator Research Organization, Tsukuba 305-0801, Japan*
[6]*Department of Physics, Kangwon National University, Chuncheon 24311, Korea*
[7]*Institut Laue-Langevin, CS 20156, 38042 Grenoble Cédex 9, France*

(Received 22 July 2020; revised 9 October 2020; accepted 10 November 2020; published 24 November 2020)

The magnetic excitations in $CoPS_3$, a two-dimensional van der Waals (vdW) antiferromagnet with Co^{2+} ion on a honeycomb lattice, have been measured using powder inelastic neutron scattering. The absence of spin-orbit exciton around 30 meV indicates that Co^{2+} ions in $CoPS_3$ have an $S = 3/2$ state rather than a spin-orbital entangled $J_{\text{eff}} = 1/2$ ground state. And, clear dispersive spin waves are observed with a large spin gap of ∼13 meV. The magnon spectra were fitted using an XXZ-type J_1-J_2-J_3 Heisenberg Hamiltonian with single-ion anisotropy assuming no magnetic exchange interaction between the honeycomb layers. The best-fit parameters show ferromagnetic exchange interactions $J_1 = -2.08$ meV and $J_2 = -0.26$ meV for the nearest- and second-nearest neighbors and a sizable antiferromagnetic exchange interaction $J_3 = 4.21$ meV for the third-nearest neighbor with the strong easy-axis anisotropy $K = -2.06$ meV. The anisotropic XXZ-type Hamiltonian could only achieve a suitable fitting. The exchange interaction for the out-of-plane spin component is smaller than that for the in-plane one by a ratio $\alpha = J_z/J_x = 0.6$. Our result directly shows that $CoPS_3$ is an experimental realization of the XXZ model with a honeycomb lattice in two-dimensional vdW magnets.

DOI: 10.1103/PhysRevB.102.184429

I. INTRODUCTION

Magnetism in two-dimensional (2D) systems has long been one of the most exciting topics in condensed-matter physics. Notably, they are the ideal playground for novel phenomena in 2D magnetic systems, such as the Berezinskii-Thouless-Kosterlitz transition of the *XY* model [1,2] and the Mermin-Wagner theorem for the Heisenberg model [3]. The recent introduction of magnetic van der Waals (vdW) materials opens enormous new and novel opportunities to examine the low-dimensional magnetism in real materials [4]. Since they are coupled by a weak vdW force along the *c* axis, it is easy to drive to the 2D limit of the bulk magnetic properties by exfoliation. These systems have so far shown various magnetic properties, including antiferromagnetic $TMPS_3$ (TM = transition metal) [5], quantum spin-liquid candidate of Kitaev magnet α-$RuCl_3$ [6,7], ferromagnetic honeycomb CrX_3 (X = Cl, Br, I) [8–11], $Cr_2Ge_2Te_6$ [12], VI_3 [13], and antiferromagnetic triangular TMX_2 family [14].

The $TMPS_3$ (TM = Mn, Fe, Co, Ni) family has attracted special interests in the community as a class of antiferromagnetic 2D vdW materials [5,15–18]. The transition-metal ions with 2+ covalency in this family form a layered honeycomb lattice with the sulfur ligand ions. They all have the same monoclinic structure with a space group $C\,2/m$, where layers on the *ab* plane are coupled by a weak vdW force along the *c* axis [16]. Since the magnetic structure and exchange interactions depend on the TM elements, they provide an excellent playground to experimentally validate spin dynamics theory in low dimensions [19–27]. For example, $FePS_3$ is described as an ideal Ising antiferromagnet [19–21,28], whereas $MnPS_3$ and $NiPS_3$ are examples of the Heisenberg model [19,22–25,29,30]. Among them, $NiPS_3$ is known to have a magnetic order close to an *XY* type [26,29]. Thickness dependence of their physical and magnetic properties has also been extensively investigated [17,26,28,30].

By comparison, $CoPS_3$ has been less studied among $TMPS_3$ due to the difficulty in synthesizing high-purity samples [27]. It is known to have an antiferromagnetic order below $T_N = 120$ K and shows a zigzag magnetic structure with the propagation vector $\boldsymbol{Q}_m = (0, 1, 0)$, as shown in Fig. 1. The Co sites' spins are aligned along the *a* axis with a small canting to the *c* axis [27]. The magnetic susceptibility shows a difference between $\mathbf{H}//ab$ and $\mathbf{H}//c$ in the paramagnetic region, which is the evidence for *XY*-like anisotropy [27]. It implies that $CoPS_3$ has anisotropic magnetic interactions depending on the magnetic moment direction.

*hoho4@snu.ac.kr
†jgpark10@snu.ac.kr

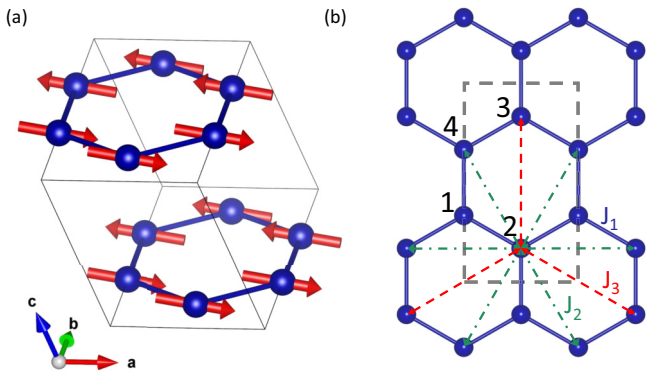

FIG. 1. (a) The magnetic structure of $CoPS_3$ with the crystallographic unit cell drawn using VESTA [49]. (b) The magnetic exchange paths are shown in the *ab* plane for the first-, second-, and third-nearest neighbors. The numbers denote the position of spins used for the spin-wave calculation.

Of further interest, the high-spin d^7 configuration in Co^{2+} compounds has recently been speculated to host a dominant Kitaev interaction as in the low-spin d^5 case for several 4 *d* and 5 *d* materials [31–34]. To realize Kitaev interaction in real materials, they need to meet two critical conditions: one is a spin-orbital entangled $J_{\text{eff}} = 1/2$ ground state and another an edge-sharing network. Since the spin-orbital state's entanglement makes exchange interactions anisotropic, having such an entangled state is particularly important to realize the Kitaev interaction [31]. In the manner of that point, the Co^{2+} system can also host the dominant Kitaev interaction via edge-shared network as it can form the spin-orbital entangled $J_{\text{eff}} = 1/2$ ground state despite small spin-orbit coupling compared to 4 *d* or 5 *d* systems. Therefore, it is worth investigating this possibility experimentally in the $CoPS_3$.

To fully understand the magnetism in $CoPS_3$, one needs to examine the underlying spin Hamiltonian in detail. Although the magnetic structure provides some information about the spin Hamiltonian, it is not sufficient to precisely determine the spin Hamiltonian. For instance, the *XY* model ($J_x = J_y, J_z = 0$) and the isotropic Heisenberg model ($J_x = J_y = J_z$) with easy-plane anisotropy can have the same magnetic ground state. Yet, their magnon spectra cannot be, *a priori*, the same for the Hamiltonian with different symmetries. Inelastic neutron scattering (INS) is the most powerful technique to measure the spin dynamics and determine the type of spin Hamiltonian and the strength of exchange interactions. INS can also be used to verify the existence of the spin-orbital entangled $J_{\text{eff}} = 1/2$ ground state by the observation of excitation from $J_{\text{eff}} = 1/2$ to $J_{\text{eff}} = 3/2$ states, which is expected to appear around 20–30 meV and used as the characteristic signature of the $J_{\text{eff}} = 1/2$ ground state in cobalt compounds [35–39].

In this paper, our INS experiment and analysis show that $CoPS_3$ has an $S = 3/2$ state instead of a $J_{\text{eff}} = 1/2$ state. And, we report the easy-plane XXZ-type spin Hamiltonian and exchange parameters of $CoPS_3$. We also compare the exchange parameters and the effect of single-ion anisotropy in $CoPS_3$ with those for other $TMPS_3$ families [20–22,24].

II. EXPERIMENTAL METHODS

Powder samples of $CoPS_3$ were synthesized by a solid-state reaction of the pure elements. Stoichiometric quantities of cobalt, phosphorus, and sulfur were placed in a quartz ampoule under an Ar atmosphere. The ingredients' total mass was 2 g, and the purity of the elements was 99.99% or better.

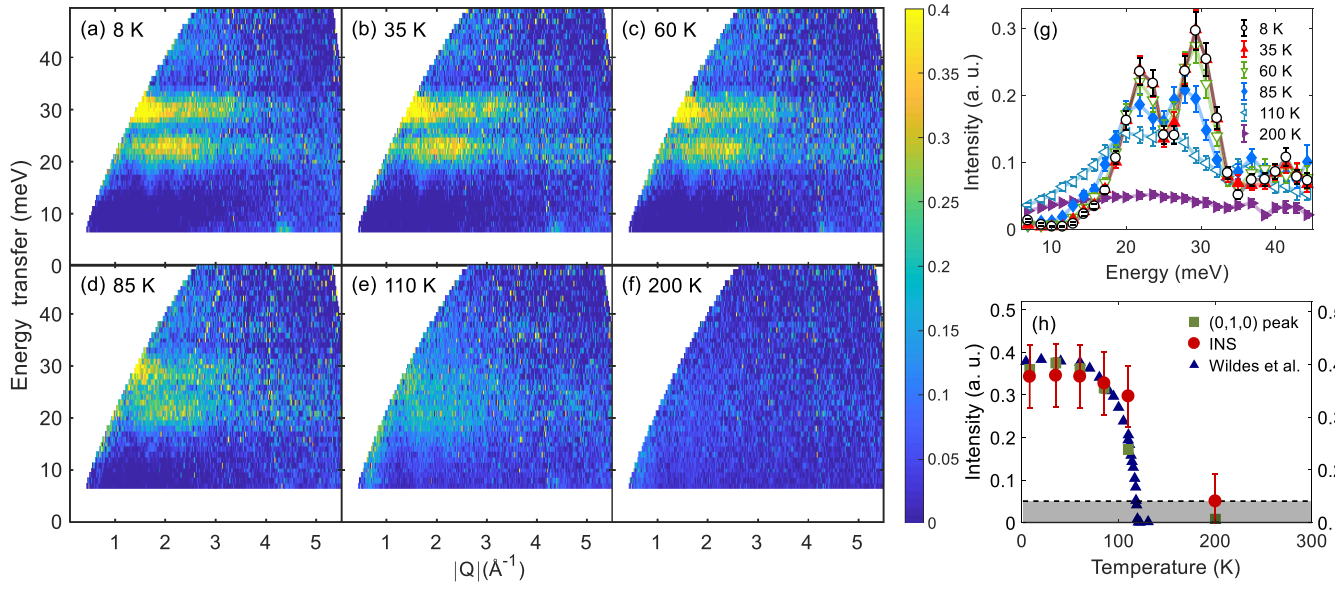

FIG. 2. (a)–(f) Magnon spectra at different temperatures. (g) Temperature dependence of magnon intensity integrated over the momentum range of $Q = [0.3, 4]$ Å^{-1}. (h) Temperature dependence of the overall integrated magnon spectra and (0,1,0) elastic peak. The blue triangle shows the integrated intensity of (0,1,0) magnetic peak in Ref. [27], and the red circle and green square show our data of magnon spectra and (0,1,0) magnetic peak each. The shaded area indicates the signals of spin fluctuations above the T_N. The reference data were scaled to compare with our data directly.

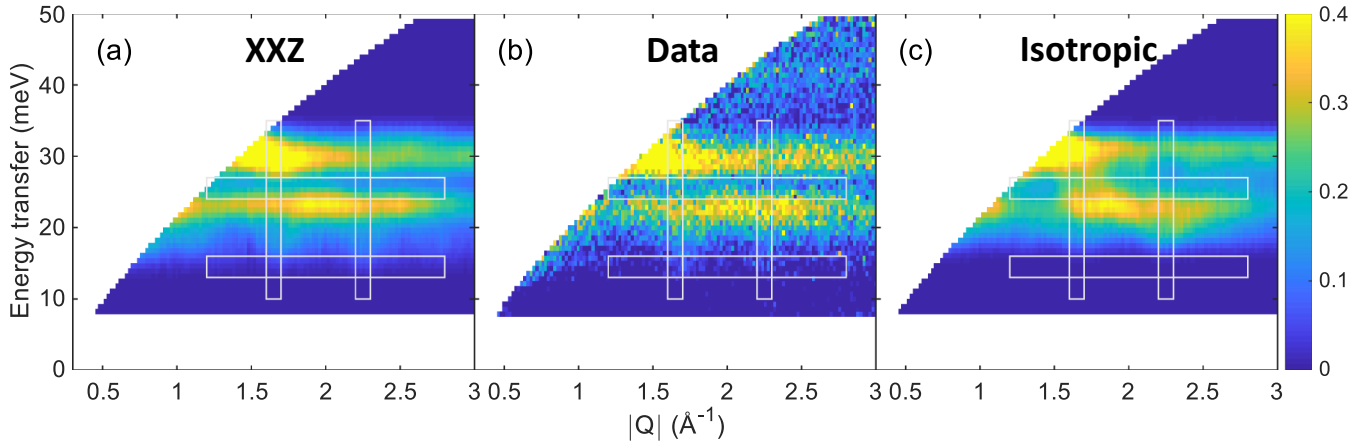

FIG. 3. (a) The best-fit magnon spectra with the XXZ model. (b) The experimental INS data of $CoPS_3$ measured at $T = 8$ K with $E_i = 71.3$ meV. (c) The best-fit magnon spectra with the isotropic Heisenberg model. An instrumental energy resolution of 3 meV was used to convolute the theoretical results shown in (a) and (c). Horizontal and vertical white boxes denote the integration range for the constant-E and constant-Q cuts in Fig. 3, respectively.

The ampoule was then evacuated, sealed under 5 Torr of argon environment, and heated in a tube furnace. The temperature was raised to 530 °C in 6 h and held there for 2 d. The quality of the sample was checked by powder x-ray diffraction and vibrating-sample magnetometer. From both measurements, we confirm the sample has an acceptable quality of the $CoPS_3$ phase.

We performed an inelastic neutron-scattering experiment using a high-resolution chopper spectrometer at J-PARC facility, Japan [40]. Taking advantage of the repetition rate multiplication method with the chopper frequency of 200 Hz, we measured the INS data at 8, 35, 60, 85, 110, and 200 K with the fixed incident neutron energies $E_i = 71.3$ and 40.3 meV. Measurements at room temperature were also carried out for the background subtraction with each incident energy. The measured INS data were reduced and binned using the MSLICE program in the DAVE suite [41]. We subtracted the room-temperature data from the data at low temperatures after applying the Bose factor to obtain pure magnon dispersions without phonon contamination.

III. RESULT

A. Absence of spin-orbital exciton

Figure 2 shows the temperature dependence of magnon dispersion with an incident neutron energy $E_i = 71.3$ meV. The phonon contamination is subtracted from the data by the same method used to analyze the 8 K data. In Figs. 2(a)–2(f), the intensity of magnon modes slowly decreases as temperature increases and dramatically collapses near the Néel temperature $T_N = 120$ K. However, there is no sign of other excitations above the Néel temperature in our data, such as dispersionless spin-orbit excitons corresponding to the transition from the $J_{eff} = 1/2$ state to the $J_{eff} = 3/2$ state. Since this excitation originates from the crystal-field splitting, it should remain above the Néel temperature. It is in stark contrast with other Co-based compounds, which exhibit flat excitations around 20–30 meV due to the magnetic excitons independent of temperature [35–39]. The absence of such excitations directly implies that $CoPS_3$ has a spin $S = 3/2$ ground state rather than the spin-orbital entangled $J_{eff} = 1/2$ ground state. So, the relating effect between the spin waves and the spin-orbit coupling, such as multilevel spin-wave theory, usually used to mix spin-orbit levels [39–41] or Kitaev interaction, cannot be applicable in this system. Therefore, in the following analysis we consider $CoPS_3$ as spin $S = 3/2$ state in the conventional linear spin-wave theory calculation.

B. Spin-wave spectrum

Figure 3 shows the spin waves taken at 8 K with an incident neutron energy $E_i = 71.3$ meV, together with representative linear spin-wave theory calculations. As one can see, the measured data show dispersive magnons with a large spin gap of ~13 meV. It shows another gap around 25 meV so that there are two magnon modes, with one being a flat upper band and another a lower dispersive one.

Most of the previous works on honeycomb lattice have used isotropic Heisenberg models. However, we found that this model does not work for $CoPS_3$ and instead used the XXZ-type (anisotropic Heisenberg) Hamiltonian with a single-ion anisotropy:

$$\mathrm{H} = \sum_{n=1}^{3} J_n \sum_{\langle i,j\rangle_n} \left[S_i^x S_j^x + S_i^y S_j^y + \alpha S_i^z S_j^z \right] + K \sum_i (\hat{x} \cdot \boldsymbol{S}_i)^2,$$

where $\alpha \in [0, 1]$ is the spin anisotropy parameter that spans from the XY model ($\alpha = 0$) to isotropic Heisenberg model ($\alpha = 1$), K is the strength of the single-ion anisotropy, and J_n is the exchange interaction up to the third-nearest neighbors. Since the interlayer interaction is presumably negligible for a weak vdW force, we ignore the interlayer coupling in our analysis. The spin-wave dispersion and powder-averaged neutron cross-section were calculated by the SPINW package [42] as well as our own analytical solutions. For our analysis, we selected the data up to $Q = 2.5$ Å^{-1}, excluding the elastic scattering below $E = 8$ meV. The difference between the simulation results and the measured data was minimized using

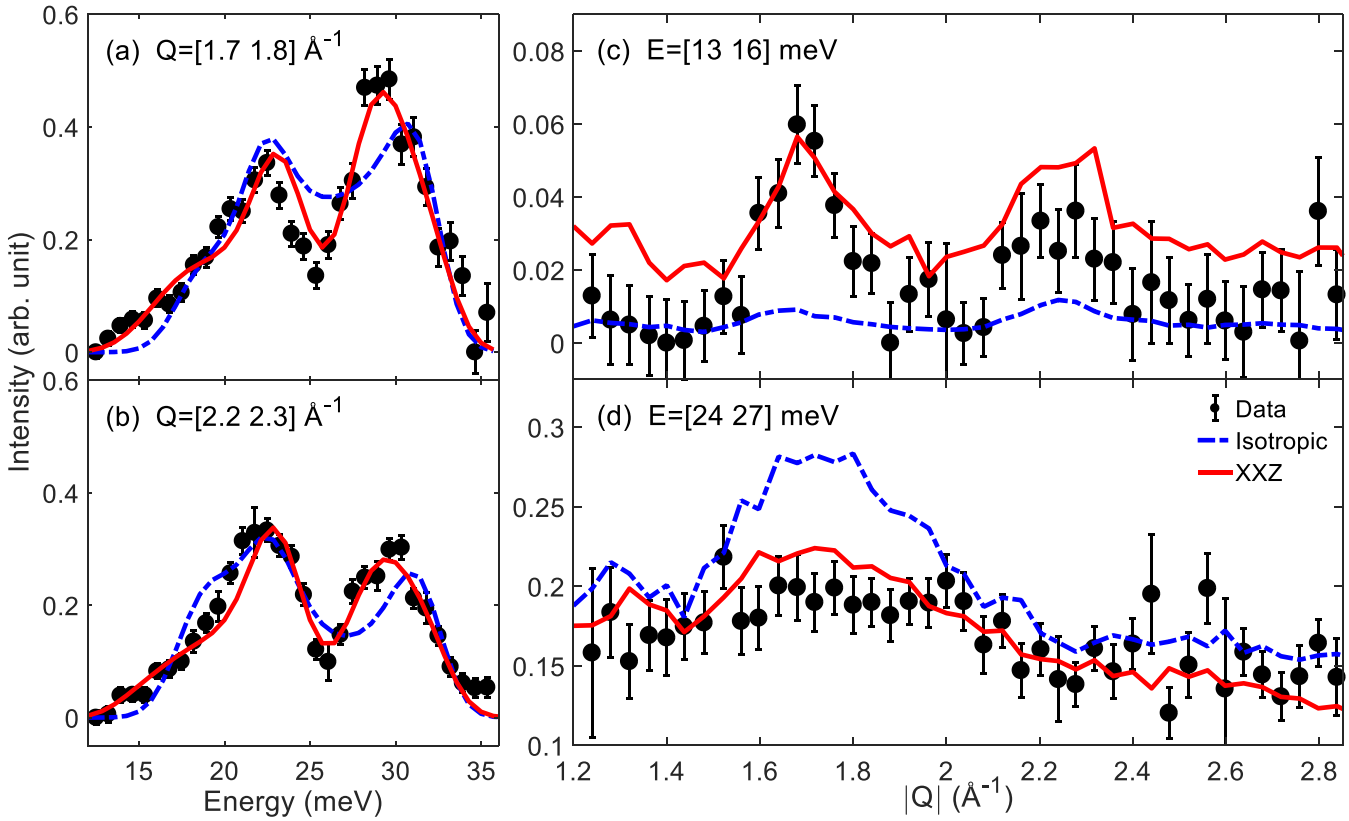

FIG. 4. (a), (b) Constant-Q cut at the momentum range of $Q = [1.7\ 1.8]$ and $Q = [2.2\ 2.3]$ Å^{-1} for the measured data with the best-fit simulations. (c), (d) Constant-E cut with the energy range of $E = [13\ 16]$ and $E = [24\ 27]$ meV. The XXZ model (solid red line) agrees better with the data.

the particle swarm optimization (PSO) algorithm [43]. The PSO algorithm is particularly adept at finding global minima in large parameter space.

Figures 3(a) and 3(c) show the simulated powder-averaged INS cross section using the best-fit parameters with the convolution of instrumental resolution of 3 meV for the XXZ-type and isotropic Heisenberg models, respectively. The best-fit parameters for the XXZ-type Heisenberg model give ferromagnetic exchange interactions for the first- and second-nearest neighbors, $J_1 = -2.08$ meV and $J_2 = -0.26$ meV, and a significant antiferromagnetic third-nearest neighbor exchange interaction $J_3 = 4.21$ meV. A strong easy-axis single-ion anisotropy $K = -2.06$ meV and planar-type spin anisotropy factor $\alpha = J_z/J_x(0.6)$ is necessary to fit the large lower spin gap, as observed in the experiments. When we tried the isotropic Heisenberg model, we found that while the sign of exchange parameters is the same as the XXZ model, their actual values are slightly changed: $J_1 = -2$, $J_2 = -0.65$, $J_3 = 3.51$, and $K = -3.62$ meV. The other key difference is the expression of the spin gaps at the zone center. Here we rewrite the formula for the spin gap for the isotropic Heisenberg model ($E_{\rm iso}$) and the XXZ-like model ($E_{\rm XXZ}$):

$$E_{\rm iso} = 2S\sqrt{-K(-K + J_1 + 4J_2 + 3J_3)},$$

$$E_{\rm XXZ} = 2S\sqrt{-K\left(-K + \frac{3\alpha - 1}{2}J_1 + (3\alpha + 1)J_2 + \frac{3\alpha + 3}{2}J_3\right)}.$$

In Fig. 4, we plot the constant-Q and constant-E cuts integrated over the range denoted in Fig. 4 with vertical and horizontal white boxes to present a detailed comparison between the two models. As clearly shown in Figs. 4(a) and 4(b), the isotropic Heisenberg model is not consistent with the low-energy gap and the extra gapped spectra at 24–27 meV. Notably, the best-fit single-ion anisotropy $K = -3.62$ meV for the isotropic model overestimates the low-energy gap. Such inconsistency is further demonstrated in Fig. 4(c); the isotropic Heisenberg model gives very small intensity in the range of energy from 13 to 16 meV around $Q = 1.7$ and 2.2 Å^{-1}. Moreover, the isotropic Heisenberg model produces a significant intensity between 24 and 27 meV. In contrast, both the INS data and the simulation from the XXZ model display the gapped feature in the same energy range.

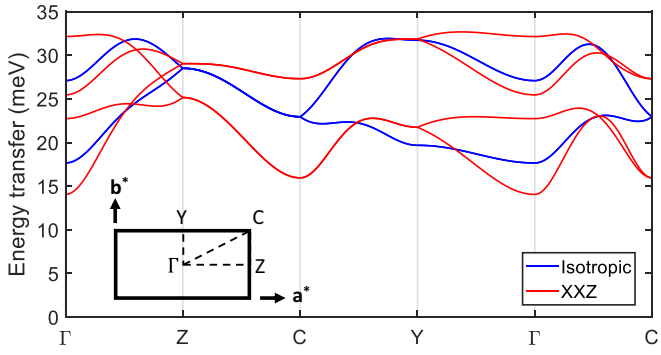

FIG. 5. The spin-wave dispersion along with the Brillouin zone's high-symmetric points for the isotropic Heisenberg model and the XXZ model. All the trajectories are given for the crystallographic unit cell. The Brillouin zone and the relevant positions are shown in the inset.

And, we would like to note that a significant portion of the original spectral weights is found to survive above the T_N due to overdamped spin waves from critical fluctuations, as shown in Figs. 2(a)–2(f). To demonstrate this point better, we plot the temperature dependence of the integrated intensity through the broad range of $Q = 0.3$–$4\,\text{Å}^{-1}$ in Figs. 2(g) and 2(h), where the signals from the high-temperature spin fluctuations are marked as the shaded area in Fig. 2(h).

IV. DISCUSSION

The magnetic structure of $CoPS_3$ that we used in the spin-wave calculation is the zigzag order with spin moments aligned to the crystallographic a axis. We accordingly set the direction of single-ion anisotropy to the a axis. From the detailed analysis of the magnetic susceptibility with crystal-field splitting, it has been suggested that the easy-axis anisotropy lies in the ac plane and is aligned along the a axis [27]. However, the actual magnetic moment direction measured by neutron diffraction has a small canting of 10.5 ° to the c axis [27]. To consider the reported structure, we also fitted the data with the canted magnetic structure as well, but the best-fit parameters and the agreement factor did not change much. The isotropic Heisenberg model is easily expected because the direction of single-ion anisotropy only forces the moment direction but does not alter the magnon spectra. In the case of the XXZ model, we had to set a larger tilting in the single-ion anisotropy to stabilize the reported canting angle due to the easy-plane spin anisotropy. However, by a similar reason to the isotropic Heisenberg model, it makes no noticeable difference.

Figure 5 shows the expected spin-wave dispersion of $CoPS_3$ along with the high-symmetry directions in the Brillouin zone, which is based on our best-fit parameter set for the isotropic Heisenberg and XXZ models, respectively. Since the spin anisotropy lowers the symmetry of the Hamiltonian, the magnon branches from the XXZ model get further split as compared to those of the isotropic Heisenberg model. Also, the magnon modes from the XXZ model are mostly well separated into two parts, and this separation makes the extra spin gap at 24–27 meV, as seen in Fig. 3(a). Moreover, the number of magnon branches is doubled over the high-symmetry lines except C-Y in the XXZ model, indicating the absence of mode degeneracy for most positions in the momentum space. We observe that the lowest nondegenerated magnon branch at 14 meV is well matched with the measured low-energy gap.

TABLE I. Magnetic exchange and anisotropy parameters for the magnetic vdW $TMPS_3$ (TM = Mn, Fe, Co, and Ni) with the parameters defined in a self-consistent way with θ is defined as the angle between the c^* axis and the vector that joins the TM ion and any particular nearest-neighbor sulfur ligand. Without trigonal distortion, θ becomes 54.7 °.

	$MnPS_3$ [22]	$FePS_3$ [20]	$CoPS_3$ (this work)	$NiPS_3$ [24]
S	5/2	2	3/2	1
T_N (K)	78	120	120	155
J_1 (meV)	1.54	−2.96	−2.04	−3.8
J_2 (meV)	0.14	0.08	−0.26	0.1
J_3 (meV)	0.36	1.92	4.21	13.8
α	1	∞	0.6	1
K (meV)	−0.0086	−2.66	−2.06	−0.3
θ (°)	51.67	51.28	51.38	51.05

In Table I, we summarize all the experimentally measured magnetic exchange parameters for the $TMPS_3$ family, with the parameters defined in a self-consistent way with including our result for $CoPS_3$ [20,22,24]. It is noticeable that despite the same crystal structure and similar antiferromagnetic order, the parameters are found to depend on the magnetic TM ion strongly. It is also noteworthy that the second-nearest neighbor exchange interaction is commonly small for all $TMPS_3$, which are supported by density-functional theory calculations as well [44].

We would now like to examine our best-fit parameters by considering magnetic properties. Using mean-field theory, we can estimate the Néel temperature T_N and the Curie-Weiss temperature Θ_{CW} as follows:

$$k_B\Theta_{CW} = -\tfrac{1}{3}S(S+1)(3J_1 + 6J_2 + 3J_3),$$
$$k_B T_N = -\tfrac{1}{3}S(S+1)(J_1 - 2J_2 - 3J_3).$$

The obtained temperatures using our best-fit parameters are found to be $\Theta_{CW} = -43.5\,\text{K}$ and $T_N = 188.5\,\text{K}$. Considering the overestimation of T_N from mean-field theory in the low-dimensional system, these values are in good agreement with the reported value of $\Theta_{CW} = -35.4\,\text{K}$ [27] and $T_N = 120\,\text{K}$. This set of parameters also stabilizes the said zigzag magnetic order [45]. Therefore, it provides further confidence in our conclusion that the parameters obtained are reasonable and agree with the bulk sample's magnetic properties.

Another interesting point is the electronic ground state of $CoPS_3$. Although the flat-like spin-orbit exciton has been observed in many cobalt compounds [35–39], $CoPS_3$ has no such excitation. Comparing with those cobalt compounds, the local environment of Co^{2+} in $CoPS_3$ has similar geometry with a distorted octahedron. The only difference between the $CoPS_3$ and other reported cobalt compounds is the type of ligand, in this case, sulfur. So, we suggest that the absence of the spin-orbital entangled state might come from the physical

effect of sulfur, such as the charge-transfer effect [46]. In fact, such different charge-transfer physics was found to play extremely interesting phenomena in $NiPS_3$ in the name of spin-charge coupling [46] and quantum entangled magnetic exciton [47].

The planar-type spin anisotropy in $CoPS_3$ can be interpreted as the consequence of the electronic configuration of Co^{2+} in the trigonally distorted octahedron. As one can see in Table I, each $TMPS_3$ compound has a very different spin-anisotropy factor α. In contrast, the angle θ, which indicates the strength of the $TMPS_3$ family's trigonal distortion, is almost identical to 51°. The only difference is the type of transition-metal elements, leading to a different electronic configuration. This different occupancy of orbital states can affect the superexchange process between the TMs. Thus, the origin of the easy-plane spin anisotropy has a close relationship with the electronic configuration of Co^{2+} and the orbital splitting by trigonal distortion.

Finally, there are several similarities in magnetism between $CoPS_3$ and $NiPS_3$. Both compounds show the zigzag antiferromagnetic order with the sizable third-nearest neighbor interaction J_3. For $NiPS_3$, the J_3 value is much larger than J_1 as $J_3/J_1 = 3$–4, which is the largest among the $TMPS_3$ family. In our analysis for $CoPS_3$, J_3 is also as large as $J_3/J_1 = 2$. Those large J_3 values are theoretically explained by a robust super-superexchange interaction between the e_g orbitals of third-neighboring Ni ions through the sulfur ligand ions [46,48]. In $NiPS_3$, two holes reside in the e_g orbitals, whereas another hole exists in t_{2g} in $CoPS_3$. This t_{2g} orbital contribution to the super-superexchange can reduce the strength of antiferromagnetic J_3. A recent study suggests that $NiPS_3$ also has easy-plane spin anisotropy [26]. Although single-ion anisotropy strength is quite different due to the difference of the electronic configuration, it is interesting that the different orbitals in $CoPS_3$ and $NiPS_3$ possess similar spin anisotropy.

V. CONCLUSION

We successfully determined the magnetic exchange parameters and the single-ion anisotropy of $CoPS_3$ using powder inelastic neutron scattering. We found that Co^{2+} in the $CoPS_3$ has a spin $S = 3/2$ state, not a spin-orbital entangled $J_{\text{eff}} = 1/2$ ground state. So, the observed magnon spectra were fitted well by the anisotropic XXZ-type J_1-J_2-J_3 Heisenberg Hamiltonian with a sizable easy-axis single-ion anisotropy of the $S = 3/2$ state. The best-fit result gives the ferromagnetic J_1 and J_2, and the antiferromagnetic J_3 exchange interactions for the first-, second-, and third-nearest neighbors in the XXZ model. We observed the large spin gap of ∼13 meV, which requires sizable single-ion anisotropy of $K = -2.06$ meV. The analysis shows that $CoPS_3$ has the XXZ-type interaction in a honeycomb lattice with an easy-plane spin anisotropy $\alpha = 0.6$. Therefore our experiment and theoretical analysis put $CoPS_3$ as another useful example of an XXZ-type honeycomb antiferromagnet. Thus, it provides an excellent playground for future investigation of low-dimensional magnetism with magnetic van der Waals materials.

ACKNOWLEDGMENTS

Work at CQM and SNU was supported by the Leading Researcher Program of the National Research Foundation of Korea (Grant No. 2020R1A3B2079375). The work at the IBS CCES was supported by the Institute of Basic Science (IBS) in Korea (Grant No. IBS-R009-G1). The INS experiment was performed at the MLF of J-PARC under a user program (Proposal No. 2019S0102).

[1] V. L. Berezinskii, Destruction of long-range order in one-dimensional and two-dimensional systems having a continuous symmetry group I. Classical systems, Sov. Phys. JETP **32**, 493 (1971).

[2] J. M. Kosterlitz and D. J. Thouless, Ordering, metastability and phase transitions in two-dimensional systems, J. Phys. C: Solid State Phys. **6**, 1181 (1973).

[3] N. D. Mermin and H. Wagner, Absence of Ferromagnetism or Antiferromagnetism in One- or Two-Dimensional Isotropic Heisenberg Models, Phys. Rev. Lett. **17**, 1133 (1966).

[4] J. G. Park, Opportunities and challenges of 2D magnetic van der Waals materials: Magnetic graphene?, J. Phys.: Condens. Matter **28**, 301001 (2016).

[5] R. Brec, Review on structural and chemical properties of transition metal phosphorous trisulfides MPS_3, Solid State Ionics **22**, 3 (1986).

[6] A. Banerjee, P. Lampen-Kelley, J. Knolle, C. Balz, A. A. Aczel, B. Winn, Y. Liu, D. Pajerowski, J. Yan, C. A. Bridges, A. T. Savici, B. C. Chakoumakos, M. D. Lumsden, D. A. Tennant, R. Moessner, D. G. Mandrus, and S. E. Nagler, Excitations in the field-induced quantum spin liquid state of α-$RuCl_3$, Npj Quantum Mater. **3**, 1 (2018).

[7] S. H. Do, S. Y. Park, J. Yoshitake, J. Nasu, Y. Motome, Y. S. Kwon, D. T. Adroja, D. J. Voneshen, K. Kim, T. H. Jang, J. H. Park, K. Y. Choi, and S. Ji, Majorana fermions in the Kitaev quantum spin system α-$RuCl_3$, Nat. Phys. **13**, 1079 (2017).

[8] C. Starr, F. Bitter, and A. R. Kaufmann, The magnetic properties of the iron group anhydrous chlorides at low temperatures. I. Experimental, Phys. Rev. **58**, 977 (1940).

[9] I. Tsubokawa, On the magnetic properties of a $CrBr_3$ single crystal, J. Phys. Soc. Jpn. **15**, 1664 (1960).

[10] B. Huang, G. Clark, E. Navarro-Moratalla, D. R. Klein, R. Cheng, K. L. Seyler, Di. Zhong, E. Schmidgall, M. A. McGuire, D. H. Cobden, W. Yao, D. Xiao, P. Jarillo-Herrero, and X. Xu, Layer-dependent ferromagnetism in a van der Waals crystal down to the monolayer limit, Nature (London) **546**, 270 (2017).

[11] T. A. Tartaglia, J. N. Tang, J. L. Lado, F. Bahrami, M. Abramchuk, G. T. McCandless, M. C. Doyle, K. S. Burch, Y. Ran, J. Y. Chan, and F. Tafti, Accessing new magnetic regimes by tuning the ligand spin-orbit coupling in van der Waals magnets, Sci. Adv. **6**, eabb9379 (2020).

[12] C. Gong, L. Li, Z. Li, H. Ji, A. Stern, Y. Xia, T. Cao, W. Bao, C. Wang, Y. Wang, Z. Q. Qiu, R. J. Cava, S. G. Louie, J. Xia, and X. Zhang, Discovery of intrinsic ferromagnetism in

two-dimensional van der Waals crystals, Nature (London) **546**, 265 (2017).

[13] S. Son, M. J. Coak, N. Lee, J. Kim, T. Y. Kim, H. Hamidov, H. Cho, C. Liu, D. M. Jarvis, P. A. C. Brown, J. H. Kim, C. H. Park, D. I. Khomskii, S. S. Saxena, and J. G. Park, Bulk properties of the van der Waals hard ferromagnet VI_3, Phys. Rev. B **99**, 041402(R) (2019).

[14] M. A. McGuire, Crystal and magnetic structures in layered, transition metal dihalides and trihalides, Crystals **7**, 121 (2017).

[15] K. S. Burch, D. Mandrus, and J. G. Park, Magnetism in two-dimensional van der Waals materials, Nature (London) **563**, 47 (2018).

[16] G. Ouvrard, R. Brec, and J. Rouxel, Structual determination of some MPS_3 layered phases (M = Mn, Fe, Co, Ni and Cd), Mater. Res. Bull. **20**, 1181 (1985).

[17] C. T. Kuo, M. Neumann, K. Balamurugan, H. J. Park, S. Kang, H. W. Shiu, J. H. Kang, B. H. Hong, M. Han, T. W. Noh, and J. G. Park, Exfoliation and raman spectroscopic fingerprint of few-layer $NiPS_3$ van der waals crystals, Sci. Rep. **6**, 20904 (2016).

[18] S. Lee, K. Y. Choi, S. Lee, B. H. Park, and J. G. Park, Tunneling transport of mono- and few-layers magnetic van der Waals $MnPS_3$, APL Mater. **4**, 086108 (2016).

[19] P. A. Joy and S. Vasudevan, Magnetism in the layered transition-metal thiophosphates MPS_3 (M = Mn, Fe, and Ni), Phys. Rev. B **46**, 5425 (1992).

[20] D. Lançon, H. C. Walker, E. Ressouche, B. Ouladdiaf, K. C. Rule, G. J. McIntyre, T. J. Hicks, H. M. Rønnow, and A. R. Wildes, Magnetic structure and magnon dynamics of the quasi-two-dimensional antiferromagnet $FePS_3$, Phys. Rev. B **94**, 214407 (2016).

[21] A. R. Wildes, K. C. Rule, R. I. Bewley, M. Enderle, and T. J. Hicks, The magnon dynamics and spin exchange parameters of $FePS_3$, J. Phys.: Condens. Matter **24**, 416004 (2012).

[22] A. R. Wildes, B. Roessli, B. Lebech, and K. W. Godfrey, Spin waves and the critical behaviour of the magnetization in $MnPS_3$, J. Phys.: Condens. Matter **10**, 6417 (1998).

[23] A. R. Wildes, H. M. Rønnow, B. Roessli, M. J. Harris, and K. W. Godfrey, Static and dynamic critical properties of the quasi-two-dimensional antiferromagnet $MnPS_3$, Phys. Rev. B **74**, 094422 (2006).

[24] D. Lançon, R. A. Ewings, T. Guidi, F. Formisano, and A. R. Wildes, Magnetic exchange parameters and anisotropy of the quasi-two-dimensional antiferromagnet $NiPS_3$, Phys. Rev. B **98**, 134414 (2018).

[25] N. Chandrasekharan and S. Vasudevan, Magnetism and exchange in the layered antiferromagnet $NiPS_3$, J. Phys.: Condens. Matter **6**, 4569 (1994).

[26] K. Kim, S. Y. Lim, J. U. Lee, S. Lee, T. Y. Kim, K. Park, G. S. Jeon, C. H. Park, J. G. Park, and H. Cheong, Suppression of magnetic ordering in XXZ-type antiferromagnetic monolayer $NiPS_3$, Nat. Commun. **10**, 345 (2019).

[27] A. R. Wildes, V. Simonet, E. Ressouche, R. Ballou, and G. J. McIntyre, The magnetic properties and structure of the quasi-two-dimensional antiferromagnet $CoPS_3$, J. Phys.: Condens. Matter **29**, 455801 (2017).

[28] J. U. Lee, S. Lee, J. H. Ryoo, S. Kang, T. Y. Kim, P. Kim, C. H. Park, J. G. Park, and H. Cheong, Ising-type magnetic ordering in atomically thin $FePS_3$, Nano Lett. **16**, 7433 (2016).

[29] A. R. Wildes, V. Simonet, E. Ressouche, G. J. McIntyre, M. Avdeev, E. Suard, S. A. J. Kimber, D. Lançon, G. Pepe, B. Moubaraki, and T. J. Hicks, Magnetic structure of the quasi-two-dimensional antiferromagnet $NiPS_3$, Phys. Rev. B **92**, 224408 (2015).

[30] K. Kim, S. Y. Lim, J. Kim, J. U. Lee, S. Lee, P. Kim, K. Park, S. Son, C. H. Park, J. G. Park, and H. Cheong, Antiferromagnetic ordering in van der Waals 2D magnetic material $MnPS_3$ probed by Raman spectroscopy, 2D Mater. **6**, 041001 (2019).

[31] G. Jackeli and G. Khaliullin, Mott Insulators in the Strong Spin-Orbit Coupling Limit: From Heisenberg to a Quantum Compass and Kitaev Models, Phys. Rev. Lett. **102**, 017205 (2009).

[32] R. Sano, Y. Kato, and Y. Motome, Kitaev-Heisenberg Hamiltonian for high-spin D7 Mott insulators, Phys. Rev. B **97**, 014408 (2018).

[33] H. Liu and G. Khaliullin, Pseudospin exchange interactions in d 7 cobalt compounds: Possible realization of the Kitaev model, Phys. Rev. B **97**, 014407 (2018).

[34] H. S. Kim, A short introduction to Kitaev magnetism: An electronic structure perspective, New Phys.: Sae Mulli **69**, 993 (2019).

[35] K. Tomiyasu, M. K. Crawford, D. T. Adroja, P. Manuel, A. Tominaga, S. Hara, H. Sato, T. Watanabe, S. I. Ikeda, J. W. Lynn, K. Iwasa, and K. Yamada, Molecular spin-orbit excitations in the $j_{\rm eff} = \frac{1}{2}$ frustrated spinel $GeCo_2O_4$, Phys. Rev. B **84**, 054405 (2011).

[36] F. Wallington, A. M. Arevalo-Lopez, J. W. Taylor, J. R. Stewart, V. Garcia-Sakai, J. P. Attfield, and C. Stock, Spin-orbit transitions in α- and γ-CoV_2O_6, Phys. Rev. B **92**, 125116 (2015).

[37] K. A. Ross, J. M. Brown, R. J. Cava, J. W. Krizan, S. E. Nagler, J. A. Rodriguez-Rivera, and M. B. Stone, Single-ion properties of the $S_{\rm eff} = \frac{1}{2}$ XY antiferromagnetic pyrochlores $NaA'Co_2F_7$ ($A' = Ca^{2+}, Sr^{2+}$), Phys. Rev. B **95**, 144414 (2017).

[38] B. Yuan, I. Khait, G.-J. Shu, F. C. Chou, M. B. Stone, J. P. Clancy, A. Paramekanti, and Y.-J. Kim, Dirac Magnons in a Honeycomb Lattice Quantum XY Magnet $CoTiO_3$, Phys. Rev. X **10**, 011062 (2020).

[39] P. M. Sarte, A. M. Arévalo-López, M. Songvilay, D. Le, T. Guidi, V. García-Sakai, S. Mukhopadhyay, S. C. Capelli, W. D. Ratcliff, K. H. Hong, G. M. McNally, E. Pachoud, J. P. Attfield, and C. Stock, Ordered magnetism in the intrinsically decorated $J_{\rm eff} = \frac{1}{2}$ α-CoV_3O_8, Phys. Rev. B **98**, 224410 (2018).

[40] S. Itoh, T. Yokoo, D. Kawana, H. Yoshizawa, T. Masuda, M. Soda, T. J. Sato, S. Satoh, M. Sakaguchi, and S. Muto, Progress in high resolution chopper spectrometer, HRC, J. Phys. Soc. Jpn. **82**, SA033 (2013).

[41] R. T. Azuah, L. R. Kneller, Y. Qiu, P. L. W. Tregenna-Piggott, C. M. Brown, J. R. D. Copley, and R. M. Dimeo, DAVE: A comprehensive software suite for the reduction, visualization, and analysis of low energy neutron spectroscopic data, J. Res. Natl. Inst. Stand. Technol. **114**, 341 (2009).

[42] S. Toth and B. Lake, Linear spin wave theory for single-q incommensurate magnetic structures, J. Phys.: Condens. Matter **27**, 166002 (2015).

[43] J. Kennedy and R. Eberhart, Particle swarm optimization, Proc. IEEE Intl. Conf. Neural Netw. **4**, 1942 (1995).

[44] B. L. Chittari, Y. Park, D. Lee, M. Han, A. H. MacDonald, E. Hwang, and J. Jung, Electronic and magnetic properties of single-layer MPX_3 metal phosphorous trichalcogenides, Phys. Rev. B **94**, 184428 (2016).

[45] J. B. Fouet, P. Sindzingre, and C. Lhuillier, An investigation of the quantum J_1-J_2-J_3 model on the honeycomb lattice, Eur. Phys. J. B **20**, 241 (2001).

[46] S. Y. Kim, T. Y. Kim, L. J. Sandilands, S. Sinn, M.-C. Lee, J. Son, S. Lee, K.-Y. Choi, W. Kim, B.-G. Park, C. Jeon, H.-D. Kim, C.-H. Park, J.-G. Park, S. J. Moon, and T. W. Noh, Charge-Spin Correlation in van der Waals Antiferromagnet $NiPS_3$, Phys. Rev. Lett. **120**, 136402 (2018).

[47] S. Kang, K. Kim, B. H. Kim, J. Kim, K. I. Sim, J.-U. Lee, S. Lee, K. Park, S. Yun, T. Kim, A. Nag, A. Walters, M. Garcia-Fernandez, J. Li, L. Chapon, K. Zhou, Y.-W. Son, J. H. Kim, H. Cheong, and J.-G. Park, Coherent many-body exciton in van der Waals antiferromagnet $NiPS_3$, Nature (London) **583**, 785 (2020).

[48] K. Takubo, T. Mizokawa, J.-Y. Son, Y. Nambu, S. Nakatsuji, and Y. Maeno, Unusual Superexchange Pathways in an NiS_2 Triangular Lattice with Negative Charge-Transfer Energy, Phys. Rev. Lett. **99**, 037203 (2007).

[49] K. Momma and F. Izumi, VESTA 3 for three-dimensional visualization of crystal, volumetric and morphology data, J. Appl. Cryst. **44**, 1272 (2011).